Journal of Zhejiang University SCIENCE A
ISSN 1673-565X (Print); ISSN 1862-1775 (Online)
www.zju.edu.cn/jzus; www.springerlink.com
E-mail: jzus@zju.edu.cn

Towards fully automatic modelling of the fracture process in quasi-brittle and ductile materials: a unified crack growth criterion*

Zhen-jun YANG, Guo-hua LIU†‡

(*College of Civil Engineering and Architecture, Zhejiang University, Hangzhou 310027, China*)

†E-mail: zjuliu@163.com

Received Oct. 8, 2007; revision accepted Feb. 25, 2008

Abstract: Fully automatic finite element (FE) modelling of the fracture process in quasi-brittle materials such as concrete and rocks and ductile materials such as metals and alloys, is of great significance in assessing structural integrity and presents tremendous challenges to the engineering community. One challenge lies in the adoption of an objective and effective crack propagation criterion. This paper proposes a crack propagation criterion based on the principle of energy conservation and the cohesive zone model (CZM). The virtual crack extension technique is used to calculate the differential terms in the criterion. A fully-automatic discrete crack modelling methodology, integrating the developed criterion, the CZM to model the crack, a simple remeshing procedure to accommodate crack propagation, the J2 flow theory implemented within the incremental plasticity framework to model the ductile materials, and a local arc-length solver to the nonlinear equation system, is developed and implemented in an in-house program. Three examples, i.e., a plain concrete beam with a single shear crack, a reinforced concrete (RC) beam with multiple cracks and a compact-tension steel specimen, are simulated. Good agreement between numerical predictions and experimental data is found, which demonstrates the applicability of the criterion to both quasi-brittle and ductile materials.

Key words: Finite element method (FEM), Crack propagation criterion, Cohesive zone model (CZM), Virtual crack extension (VCE), Arc-length method

doi:10.1631/jzus.A071540 **Document code:** A **CLC number:** O34; TV3

INTRODUCTION

The fracture process in different materials such as concrete and rocks, metals and alloys subjected to fracture has been heavily investigated, both experimentally and numerically, to quantify the facture resistance of engineering structures. Whereas the experimental studies are indispensable in obtaining insights into the basic mechanisms of the fracture process, numerical modelling methods such as the finite element method (FEM) and the boundary element method, are playing a more and more important role in understanding the full mechanical behavior of complex engineering structures, because of their great flexibility and wide applicability.

Experiments indicate that crack propagation in quasi-brittle and ductile materials is governed by different physical mechanisms. In concrete, e.g., cracks form by intersection and coalescence of micro-cracks and flaws at the interfaces between aggregates and inclusions in a narrow band termed the fracture process zone (FPZ) at the fracture front (Hillerborg and Rots, 1989), while in ductile materials cracks form by nucleation, growth and coalescence of micro-voids (Gurson, 1977; Zhang *et al*., 2000). A common feature of the fracture process in these ma-

‡ Corresponding author

* Project supported by the Scientific Research Foundation for Returned Overseas Chinese Scholars, MOE (No. J20050924), and the United Research Foundation of the National Natural Science Committee and the Ertan Hydropower Development Co. Ltd., China (No. 50579081)

terials is that cracking is accompanied with gradual energy dissipation in FPZ as the crack opens. The difference is that outside FPZ, the concrete behaves almost linear-elastically whereas the ductile materials experience small-scale or large-scale plastic yielding. Since classic elasticity and plasticity theories have been long established as well as their numerical implementation in finite element method (FEM), successful modelling of fracture behaviour in both materials is now very much dependent upon accurate modelling of FPZ.

Two types of constitutive models are now widely used to simulate the microscopic separation mechanism in FPZ: the cohesive zone models (CZMs) and crack band models (CBMs). It may be noted that CZMs are more frequently termed cohesive crack models or fictitious crack models for concrete as originally proposed by Hillerborg *et al.*(1976). The CZMs are often implemented by nodal force release procedures or, more generally, by nonlinear cohesive interface elements (CIEs) with zero initial thickness, whose constitutive relations are characterized by transferred tractions versus crack surface relative displacement relations (e.g., Bocca *et al.*, 1991; Rots, 1991; Xie and Gerstle, 1995; Tvergaard and Hutchinson, 1992; 1996; Siegmund and Brocks, 2000; Li and Siegmund, 2002; Li and Chandra, 2003). The CBMs model the FPZ with continuum elements with a fixed thickness. Accordingly, two types of crack models are widely used to implement the constitutive models for FPZ, i.e., discrete crack models and smeared crack models. In modelling single tensile crack propagation in plain concrete beams, both discrete and smeared models are able to satisfactorily predict crack trajectories and load-displacement responses (Yang and Proverbs, 2004). However, both have only achieved limited success in modelling multiple distributed crack propagation in concrete structures such as reinforced concrete (RC) beams, with the smeared crack model being far more popular because of its computational convenience (ACI Report 446.3R-97, 1997). It may be noted that discrete crack models have distinct advantages over smeared models where information such as the detailed cracking path, crack spacing and crack width are of interest. Modelling ductile fracture is far less developed than modelling quasi-brittle fracture because of the extra complexities related to the material plasticity. Most of the existing finite element (FE) simulations of ductile crack propagation, either using CZMs or CBMs, modelled Mode-I fracture in symmetric specimens subjected to symmetric loading conditions. In these cases the cracking path is a priori (along the structural symmetry line) and thus interface elements in CZMs or void-containing cell elements in CBMs can be pre-inserted in FE meshes. The surface energy dissipation is then modelled by a gradual strain softening of these elements. In this way there is no need to judge when and in which direction a crack will propagate, i.e., an explicit crack propagation criterion is not needed. This, however, comes with high computational demands and restrictions in modelling practical fracture problems often subjected to complex loading conditions.

This paper proposes an explicit crack propagation criterion, based on the Griffith energy concept and the CZM, with a view to developing an effective and efficient FE tool for fully automatic modelling of crack propagation in practical structures made up of different materials. The purposes of this paper are: (1) to present the criterion and discuss its wide applicability in the sense that it can be used to model fracture behaviour in quasi-brittle and ductile materials; (2) to implement the criterion in the finite element context so that a unified numerical framework can be used for modelling fracture in the above materials. This should be conceptually an important advance, considering that the existing numerical simulations of crack propagation in different materials are mostly carried out separately by different numerical models; (3) to validate the criterion by modelling typical examples with well-documented experimental data. The paper first presents in detail the derivation of the proposed criterion. A fully automatic modelling methodology of crack propagation is then briefly described. Three examples, i.e., a plain concrete beam with a single mixed-mode crack, a reinforced concrete beam with multiple cracks and a compact-tension steel specimen are then modelled and the numerical results are discussed.

DERIVATION OF THE CRITERION

The fundamental principle of energy conservation with respect to unit area crack extension, based

on which Griffith (1921) developed the first fracture mechanics criterion, can be mathematically stated as:

$$T_r = \frac{\partial}{\partial A}(W_F - U_e - U_p - E_s)$$
$$\begin{cases} > 0, & \text{when crack propagates,} \\ = 0, & \text{when the critical condition,} \\ < 0, & \text{when crack does not propagate,} \end{cases} \quad (1)$$

where U_e and U_p are the elastic strain energy and the plastic strain energy of the system, respectively. W_F is the work done by the externally applied loadings, E_s is the surface dissipated energy and A is the total crack surface area. The result of the first two terms in Eq.(1) is the strain energy release rate which can be regarded as a driving force of crack growth G:

$$G = \frac{\partial(W_F - U_e)}{\partial A}. \quad (2a)$$

The last two terms represent the plastic energy dissipation rate and the energy dissipation rate due to crack surface separation. The summation of them represents the crack growth resistance, which is termed "energy dissipation rate" R in (Turner and Kolednik, 1994; Siegmund and Brocks, 2000; Li and Chandra, 2003)

$$R = \frac{\partial(U_p + E_s)}{\partial A}. \quad (2b)$$

Therefore, Eq.(1) shows that when the crack driving force exceeds the crack resistance force, the crack will propagate.

A planar system subjected to surface traction vector $\boldsymbol{t}$ and body force vector $\boldsymbol{b}$ with a propagating crack is illustrated in Fig.1. The crack is represented by the CZM characterized by the tangential traction $\boldsymbol{\sigma}$ vs crack opening displacement (COD) relation and the shear stress $\boldsymbol{\tau}$ vs crack sliding displacement (CSD) relation. The plastic zone shown in Fig.1 is only for illustration.

The differentiation in Eq.(1) can be evaluated numerically by various methods in an elastic-plastic context such as line contour integration, continuum area integration, virtual crack extension (VCE) methods and direct evaluation of the potential energy change due to a small crack extension. The VCE (Hellen, 1975) is used in this study.

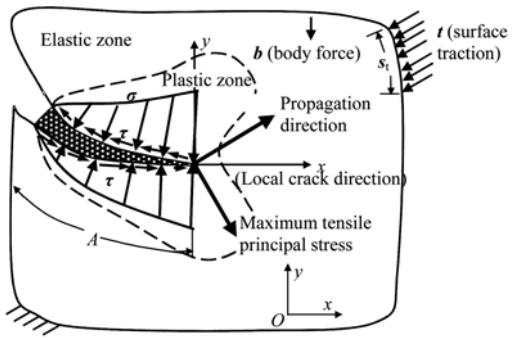

Fig.1 Planar elastic-plastic system subjected to mixed-mode fracture

In the context of the FEM, the external work and the total strain energy of the system U can be expressed respectively as:

$$W_F = \boldsymbol{u}^T \boldsymbol{F}, \quad (3a)$$

$$U = U_e + U_p = \int_V W \mathrm{d}V, \quad (3b)$$

where V is the system volume, $\boldsymbol{u}$ the nodal displacement vector, $\boldsymbol{F}$ the nodal equivalent force vector and W the total strain energy density. The volume integration in Eq.(3b) can be carried out in an element-by-element way. The strain energy of each element is calculated first using the Gauss quadrature and then a summation is carried out for all the elements as

$$U = \sum_{NE} \sum_{j=1}^{2} \sum_{k=1}^{2} \left\{ J(\eta_j, \xi_k) \cdot W(\eta_j, \xi_k) \right\}. \quad (4)$$

A 2×2 Gauss quadrature is used in Eq.(4). NE is the total element number. $W(\eta_j, \xi_k)$ is the strain energy density at the Gauss point (j, k) of an element where η_j and ξ_k are the isoparametric coordinates of this Gauss point. $J(\eta_j, \xi_k)$ is the product of the weighting factor and the determinant of the element Jacobian matrix at the Gauss point (j, k). The strain energy density can be expressed as (the indices in the parenthesis for $J(\eta_j, \xi_k)$ and $W(\eta_j, \xi_k)$ are dropped for simplification thereafter):

$$W=\int_0^{\varepsilon_{mn}}\boldsymbol{\sigma}^{\mathrm{T}}\mathrm{d}\boldsymbol{\varepsilon}, \tag{5}$$

where $\boldsymbol{\sigma}$ and $\boldsymbol{\varepsilon}$ are stress and strain vectors at a Gauss point, respectively. $\boldsymbol{\varepsilon}_{\mathrm{mn}}$ is the strain vector of current iterative step. For a non-linear elastic material behaviour, or an elastic-plastic one under proportional loading,

$$\frac{\partial W}{\partial A}=\frac{\partial W}{\partial \boldsymbol{\varepsilon}}\frac{\partial \boldsymbol{\varepsilon}}{\partial A}=\boldsymbol{\sigma}^{\mathrm{T}}\frac{\partial \boldsymbol{\varepsilon}}{\partial A}. \tag{6}$$

Substituting Eqs.(3)~(6) into Eq.(1) leads to

$$\begin{aligned}T_{\mathrm{r}}=&-\frac{\partial E_{\mathrm{s}}}{\partial A}-\sum_{NE}\sum_{j=1}^{2}\sum_{k=1}^{2}\left\{\frac{\partial J}{\partial A}W+J\boldsymbol{\sigma}^{\mathrm{T}}\frac{\partial \boldsymbol{\varepsilon}}{\partial A}\right\}\\&+\frac{\partial \boldsymbol{u}^{\mathrm{T}}}{\partial A}\boldsymbol{F}+\boldsymbol{u}^{\mathrm{T}}\frac{\partial \boldsymbol{F}}{\partial A}.\end{aligned} \tag{7}$$

Considering a small deformation we have

$$\frac{\partial \boldsymbol{\varepsilon}}{\partial A}=\frac{\partial(\boldsymbol{B}\boldsymbol{u})}{\partial A}=\frac{\partial \boldsymbol{B}}{\partial A}\boldsymbol{u}+\boldsymbol{B}\frac{\partial \boldsymbol{u}}{\partial A}, \tag{8}$$

where $\boldsymbol{B}$ is the strain matrix. Substituting Eq.(8) into Eq.(7) and noticing that the last term of Eq.(7) is zero, because the applied external loads do not change with the VCE, we have

$$\begin{aligned}T_{\mathrm{r}}=&-\frac{\partial E_{\mathrm{s}}}{\partial A}-\sum_{NE}\sum_{j=1}^{2}\sum_{k=1}^{2}\left\{\frac{\partial J}{\partial A}W+J\boldsymbol{\sigma}^{\mathrm{T}}\frac{\partial \boldsymbol{B}}{\partial A}\boldsymbol{u}\right\}\\&+\frac{\partial \boldsymbol{u}^{\mathrm{T}}}{\partial A}\left[\sum_{NE}\sum_{j=1}^{2}\sum_{k=1}^{2}\left\{J\boldsymbol{\sigma}^{\mathrm{T}}\boldsymbol{B}\right\}+\boldsymbol{F}\right].\end{aligned} \tag{9}$$

The first term in Eq.(9), i.e., the surface energy dissipation rate, can be expressed as (Xie and Gerstle, 1995)

$$\frac{\partial E_{\mathrm{s}}}{\partial A}=\int\frac{\partial \boldsymbol{d}_{\mathrm{r}}}{\partial A}\boldsymbol{s}_{\mathrm{t}}\,\mathrm{d}A, \tag{10}$$

where $\boldsymbol{d}_{\mathrm{r}}=[COD, CSD]^{\mathrm{T}}$ is the relative displacement vector of the crack surface and $\boldsymbol{s}_{\mathrm{t}}=[\boldsymbol{\sigma}, \boldsymbol{\tau}]^{\mathrm{T}}$ is the transferred stress vector. Fig.2 illustrates using two four-node CIEs to model the FPZ. These CIEs are special in that they use linear $\boldsymbol{d}_{\mathrm{r}}$ distribution along their length and nonlinear $\boldsymbol{s}_{\mathrm{t}}$ distribution (Xie, 1995). Relating $\boldsymbol{d}_{\mathrm{r}}$ with the global nodal displacements by a linear shape function matrix $\boldsymbol{M}$ yields

$$\begin{aligned}\frac{\partial E_{\mathrm{s}}}{\partial A}&=\int\frac{\partial(\boldsymbol{M}^{\mathrm{T}}\boldsymbol{u})}{\partial A}\boldsymbol{s}_{\mathrm{t}}\mathrm{d}A=\int\left[\boldsymbol{u}^{\mathrm{T}}\frac{\partial \boldsymbol{M}}{\partial A}+\frac{\partial \boldsymbol{u}^{\mathrm{T}}}{\partial A}\boldsymbol{M}\right]\boldsymbol{s}_{\mathrm{t}}\mathrm{d}A\\&=\boldsymbol{u}^{\mathrm{T}}\int\frac{\partial \boldsymbol{M}}{\partial A}\boldsymbol{s}_{\mathrm{t}}\mathrm{d}A+\frac{\partial \boldsymbol{u}^{\mathrm{T}}}{\partial A}\int\boldsymbol{M}\boldsymbol{s}_{\mathrm{t}}\mathrm{d}A.\end{aligned} \tag{11}$$

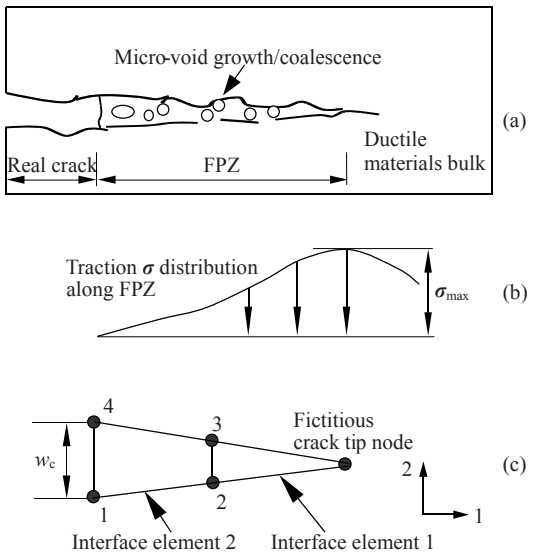

Fig.2 Modelling of FPZ in ductile materials with 4-node cohesive interface elements. (a) Real crack and FPZ at the fracture front; (b) Traction σ distribution along FPZ; (c) 4-node cohesive interface elements for FPZ

Substituting Eq.(11) into Eq.(9) we have

$$\begin{aligned}T_{\mathrm{r}}=&-\sum_{NE}\sum_{j=1}^{2}\sum_{k=1}^{2}\left\{\frac{\partial J}{\partial A}W+J\boldsymbol{\sigma}^{\mathrm{T}}\frac{\partial \boldsymbol{B}}{\partial A}\boldsymbol{u}\right\}-\boldsymbol{u}^{\mathrm{T}}\int\frac{\partial \boldsymbol{M}}{\partial A}\boldsymbol{s}_{\mathrm{t}}\mathrm{d}A\\&+\frac{\partial \boldsymbol{u}^{\mathrm{T}}}{\partial A}\left[\sum_{NE}\sum_{j=1}^{2}\sum_{k=1}^{2}\left\{J\boldsymbol{\sigma}^{\mathrm{T}}\boldsymbol{B}\right\}+\boldsymbol{F}-\int\boldsymbol{M}\boldsymbol{s}_{\mathrm{t}}\mathrm{d}A\right].\end{aligned} \tag{12}$$

The last term in the bracket is the difference between the internal and external forces and should be zero when an equilibrium state is established. Therefore the energy criterion for ductile crack propagation becomes

$$-\sum_{NE}\sum_{j=1}^{2}\sum_{k=1}^{2}\left\{\frac{\partial J}{\partial A}W+J\boldsymbol{\sigma}^{\mathrm{T}}\frac{\partial \boldsymbol{B}}{\partial A}\boldsymbol{u}\right\}-\boldsymbol{u}^{\mathrm{T}}\int\frac{\partial \boldsymbol{M}}{\partial A}\boldsymbol{s}_{\mathrm{t}}\mathrm{d}A$$

$$\begin{cases} > 0, & \text{when crack propagates,} \\ = 0, & \text{when the critical condition,} \\ < 0, & \text{when crack does not propagate,} \end{cases} \quad (13)$$

One can notice that when deriving the criterion, no assumptions are made on the fracture mode and the size of the plasticity zone. Thus the criterion is applicable for both Mode-I and mixed-mode fracture problems involving either small-scale or large-scale yielding. Although Fig.1 illustrates the planar system, the derivation for 3D problems is virtually identical except that 3D surface CIEs should be used to model the CZM. The limitation of this criterion is that in deriving Eq.(6), a non-linear elastic material behaviour, or an elastic-plastic one under proportional loading (without unloading), must be assumed.

For quasi-brittle fracture where the bulk material behaves linear-elastically, the first term in Eq.(13) can be explicitly expressed by the stiffness matrices of FEs and this criterion reduces to the criterion originally derived by Xie and Gerstle (1995) as

$$-\frac{1}{2}\boldsymbol{u}^{\mathrm{T}}\frac{\partial \boldsymbol{K}}{\partial A}\boldsymbol{u}-\boldsymbol{u}^{\mathrm{T}}\int\frac{\partial \boldsymbol{M}}{\partial A}\boldsymbol{s}_{\mathrm{t}}\mathrm{d}A \begin{cases} > 0, & \text{when crack propagates,} \\ = 0, & \text{when the critical condition,} \\ < 0, & \text{when crack does not propagate,} \end{cases} \quad (14)$$

where $\boldsymbol{K}$ is the total stiffness matrix of the elastic bulk. Eqs.(13) and (14) can then be calculated using a finite difference procedure with a virtual crack extension ΔA. The simplest VCE is to move only the crack-tip elements so only crack-tip elements contribute to Eqs.(13) and (14) (Xie and Gerstle, 1995) and their evaluation becomes trivial.

FULLY AUTOMATIC DISCRETE CRACK MODELLING METHODOLOGY

Fully automatic simulations of discrete crack propagation based on CZM in practical problems (e.g., RC beams) need a number of highly sophisticated constitutive models and corresponding numerical models, and a set of numerical algorithms to solve equation systems with high nonlinearity resulting from coupling of material plasticity, strain-softening of interface elements representing cracks and continuous boundary changes. The most critical components may include: the constitutive law for CZM simulating the strain-softening of nonlinear CIEs, the crack propagation criterion, the remeshing procedure to change the FE mesh to accommodate crack propagation, the mesh-mapping techniques to transfer structural responses from old FE meshes to new ones, and the numerical algorithms to solve the nonlinear equation systems. Fig.3 shows a very simplified flowchart in automatic modelling of discrete cohesive crack propagation. Once the criterion Eq.(13) or Eq.(14) is met, a CIE is automatically inserted in the propagating direction and all the topological information of the FE mesh is correspondingly changed. The crack is assumed to propagate in the direction perpendicular to the principal tensile stress at the crack tip. A local normal plane arc-length constraint method (May and Duan, 1997) and the modified Newton-Raphson iterative procedure are used to solve the nonlinear equation system. Readers are referred to a previous study (Yang and Chen, 2004) for further information.

The associated J2 flow theory (von Mises yielding criterion) with an isotropic hardening is implemented within the incremental plasticity framework to model the constitutive behaviour of the

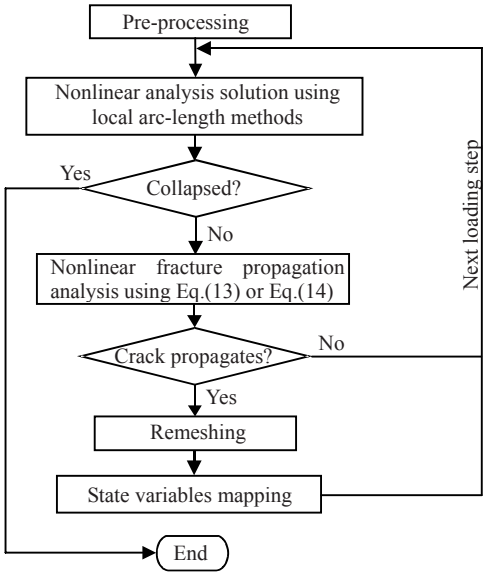

Fig.3 Simplified flowchart of automatic cohesive crack propagation using FEM

ductile materials. It should be noted that when the incremental plasticity with J2 flow theory is used, unloading is not allowed, otherwise Eq.(6) will be invalidated.

NUMERICAL EXAMPLES, RESULTS AND DISCUSSION

The first example is the four-point single-edge notched shear (SENS) beam which is first tested and analysed by Arrea and Ingraffea (1982). This shear beam has since become a benchmark for the purpose of mixed-mode crack propagation analysis using FEM (Rots and de Borst, 1987; Xie and Gerstle, 1995). Its geometry, boundary conditions and material properties are shown in Fig.4. The constitutive law of the nonlinear CIEs, i.e., the normal traction vs crack opening displacement (σ-COD) curve, is represented by Petersson (1981)'s bilinear model as shown in Fig.5. The concrete has Young's modulus 24.8 GPa, Poisson's ratio 0.18 and tensile strength f_t=4.0 MPa. The following parameters are obtained

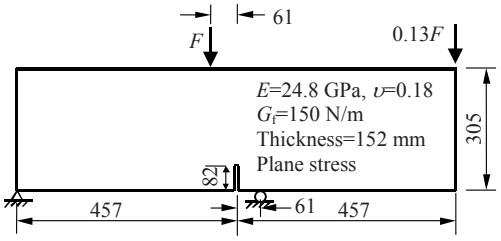

Fig.4 SENS beam for mixed-mode crack propagation (unit: mm)

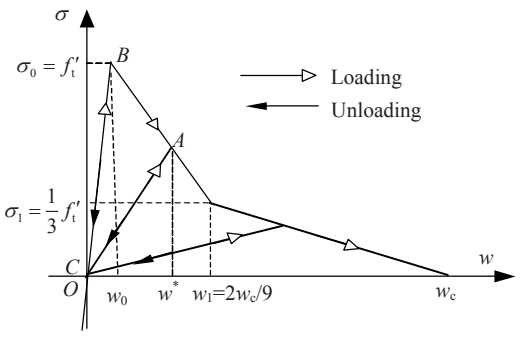

Fig.5 Petersson's bilineare σ-COD curve for quasi-brittle fracture

from the fracture energy G_f=150 N/m which is the area under the σ-COD curve: $\sigma_0=f_t$=4.0 MPa, w_c=0.135 mm, σ_1=1.33 MPa and w_1=0.03 mm. The value of w_0 is assumed as 0.0001 mm with a high initial stiffness k_0=40000 MPa/mm. A plane stress condition is assumed.

Fig.6a shows the initial FE mesh and Figs 6b~6e illustrate the cracking process of the beam, which is fully automatically modelled by the discrete crack modelling approach. The predicted cracking processes and the curved crack trajectories are in very good agreement with the experimental observations. One can see that during the simulation, the FE meshes are gradually refined around the cracks as they propagate. Fig.6f compares the predicted load vs crack mouth sliding displacement (CMSD) curves with the experimental data. Again excellent agreements can be seen.

A simply supported RC beam OA-2 tested under a concentrated load at the mid-span by Bresler and Scordelis (1963) is modeled as the second example. It has a length of 5029 mm with a shear span of 4572 mm and a cross-section of 305 mm×559 mm (12 in×22 in) (Fig.7). It is reinforced with five 9# high strength deformed steel bars with a total nominal cross-sectional area of 3290 mm^2 at an effective depth of 466 mm. The beam is not reinforced with stirrups. The concrete has the following parameters: Young's modulus E=24.0 GPa, the tensile strength f_t=2.37 MPa and the fracture energy G_f=100 N/m. The use of the same bilinear softening law (Fig.5) leads to the following parameters for CIEs: $\sigma_0=f_t$=2.37 MPa, w_c=0.152 mm, σ_1=0.79 MPa and w_1=0.034 mm. The value of w_0 is assumed as 0.0001 mm with a high initial stiffness k_0=2400 MPa/mm. The steel bars have Young's modulus 200 GPa and average yield strength 552 MPa. The Poisson's ratios for the concrete and the steel bars are assumed here to be 0.18 and 0.3, respectively. A plane stress condition is assumed for the analysis. Only half of the beam is modeled considering symmetry. Fig.8a shows an initial FE mesh modeled for this RC beam. A special type of tension-softening elements is used to model the bon-slip behavior between the reinforcing bars and the surrounding concrete. Interested readers are referred to (Xie, 1995) for a full description of this type of elements.

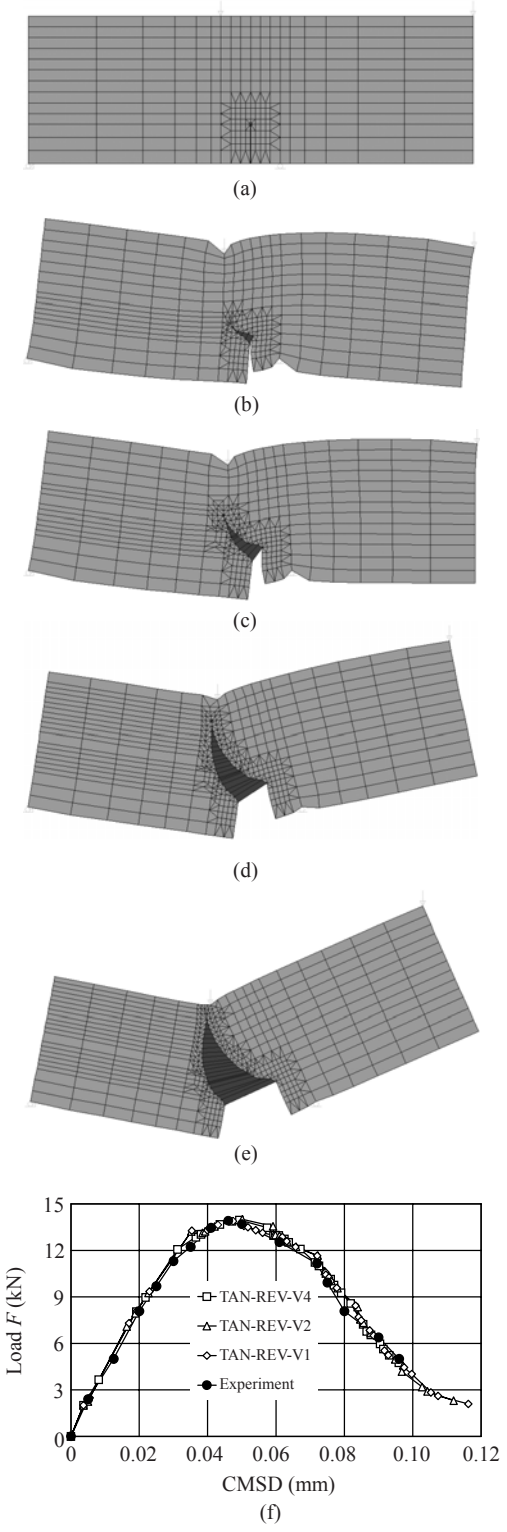

Fig.6 Modelling single crack propagation in the beam SENS (displacement display scale=500). (a) Initial FE mesh; (b) *F*=140 kN (peak load); (c) *F*=120 kN; (d) *F*=60 kN; (e) *F*=20 kN (on collapse): 519 nodes and 25 interface elements; (f) Load-CMSD curves

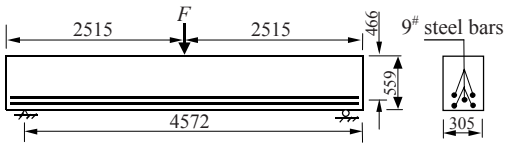

Fig.7 RC beam OA-2 for multiple crack propagation modelling (unit: mm)

Figs.8b~8f illustrate the cracking process of the beam, which was modeled fully automatically using the presented discrete crack model. The dotted lines are truss elements representing all the five steel bars. The predicted cracking process in general agrees well with experimental observations. It can be seen that the FE mesh has significantly changed in Figs.8b~8f from the initial mesh (Fig.8a). The numbers of elements, nodes and interface elements increase from 410, 420 and 0 to 926, 696 and 115, respectively. It is remarkable that the adopted remeshing procedure can adapt such dramatic changes. Fig.9a shows the test crack pattern (Bresler and Scordelis, 1963). This may be compared with the predicted one as shown in Fig.9b which is the same as that in Fig.8f except that the undeformed mesh is shown here. Within the shear span, the model predicted 17 cracks (a number of which may be still too small to be seen in a real test) compared with 13 observed in the test. Fig.10 shows the predicted load vs deflection relationship at the mid-span using the Strong Bond assumption. Test results are also shown for comparison. It can be seen that the prediction is in very close agreement with the test data for loading up to about 285 kN. Beyond this point the stiffness of the beam is slightly over-predicted. This is inevitable because the plasticity of concrete under compression and compression cracking has not been considered in the current model.

The third example is a compact tension specimen tested by Dhar *et al.*(2000). Fig.11 shows its geometry and dimensions. The specimen is made up of AISI-1095 spheroidized steel. Its Young's modulus, Poisson's ratio, yield strength σ_y, ultimate strength and ultimate strain, obtained from a tension test, are 210 GPa, 0.3, 497 MPa, 690 MPa and 0.15, respectively. A corresponding curve with a linear hardening modulus of about 1300 MPa is used as the effective plastic strain vs stress relation. A tri-linear σ-COD relation shown in Fig.12 is assumed as the constitutive law of the CIEs. The critical *J*-integral to

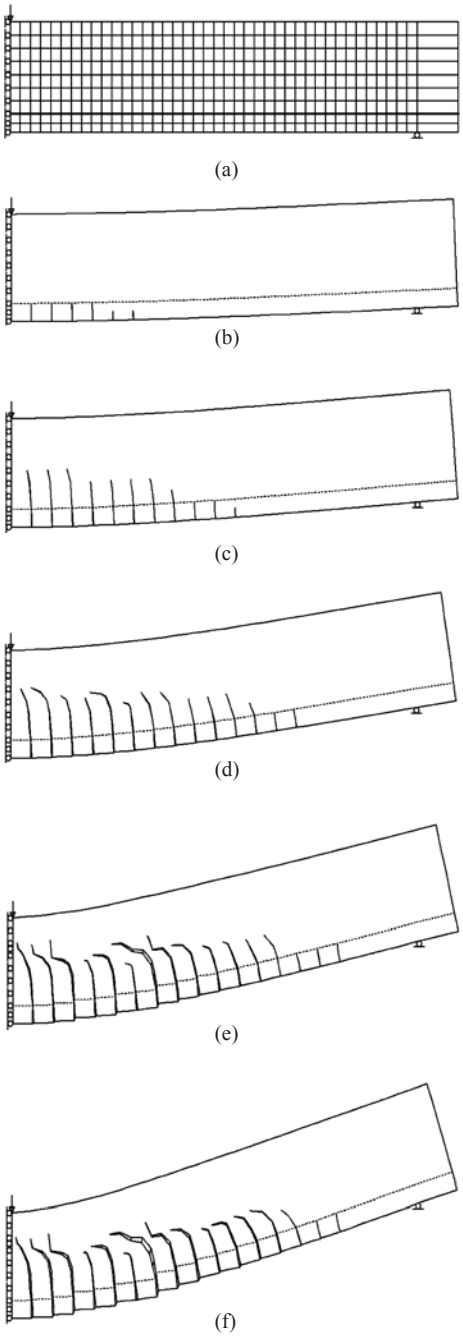

Fig.8 Modelling multiple crack propagation in the RC beam OA-2 (displacement display scale=50). (a) Initial FE mesh, 410 elements and 420 nodes; (b) *F*=73 kN, 484 nodes and 515 elements with 16 interface elements; (c) *F*=115 kN, 552 nodes and 655 element with 51 interface elements; (d) *F*=200 kN, 618 nodes and 790 elements with 81 interface elements; (e) *F*=285 kN, 693 nodes and 962 elements with 111 interface elements; (f) *F*=358 kN, 696 nodes and 926 elements with 115 interface elements

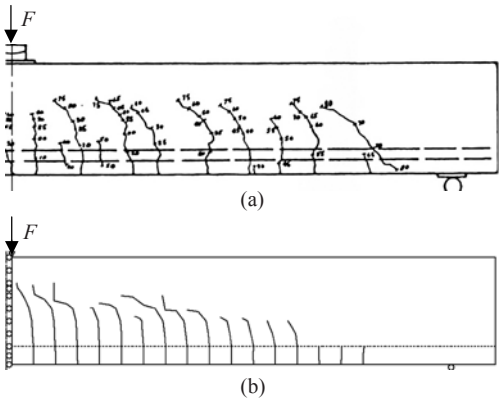

Fig.9 Crack patterns at failure of the RC beam OA-2. (a) Test result (south face); (b) Predicted result

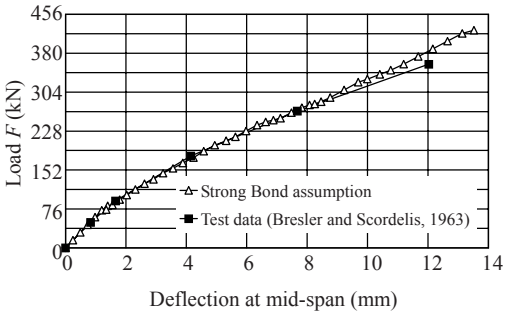

Fig.10 Predicted load vs deflection curve of the RC beam OA-2

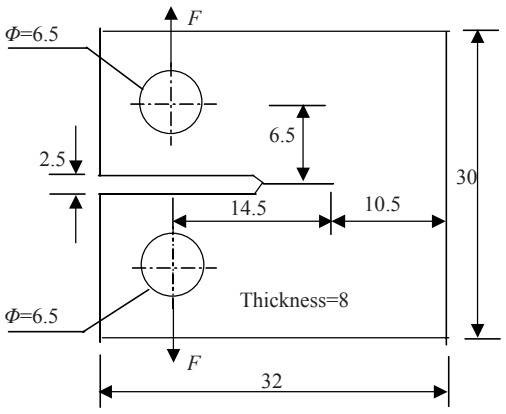

Fig.11 CT steel specimen (unit: mm)

initiate a crack is 65 N/mm for the specimen (Dhar *et al.*, 2000). This value is assumed as the area under the σ-COD relation. The following parameters in Fig.12 are used: the cohesive strength σ_{max}=750 MPa, δ_c=0.116 mm and δ_2=0.058 mm. δ_1 is assumed 0.001 mm to give a high initial stiffness of CIEs.

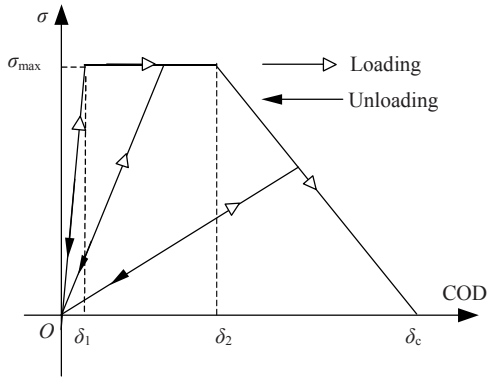

Fig.12 Tri-linear σ-COD curve for ductile fracture

A plane strain condition is assumed. Because the method of pre-inserting CIEs on the cracking line does not involve an explicit crack growth criterion, its results should be solely determined by the assumed σ-COD relation for a given FE mesh. This method is therefore used and the results are compared with those from the automatic modelling methodology. Fig.13 shows a typical FE mesh with pre-inserted CIEs (Mesh *P*). Three initial FE meshes without pre-inserted CIEs, i.e., Mesh 1, Mesh 2 and Mesh 3 shown in Fig.14, whose densities differ mainly around the cracking line, are designed to investigate the mesh objectivity of the proposed criterion.

Fig.15 shows the evolutions of the cohesive crack zone and plasticity zone simulated by the automatic modelling approach using Mesh 2. In the several cracking steps of the early stage, no plasticity occurs in the bulk material. This is perhaps because the assumed cohesive strength σ_{max}=750 MPa is so low that the surface separation accounts for most of the dissipated energy. This is also noticed by Li and Chandra (2003). Different σ-COD relations may lead to dramatically different pictures. One can also see large-scale yielding appear in the later stages. A good similarity is seen between the evolutions of the cohesive crack zone and plasticity zone simulated from Mesh *P*, Mesh 1 and Mesh 2. Modelling of the finest mesh Mesh 3 fails to reach the peak load due to divergence.

Fig.16 shows the load-load point deflection curves from the test and the FE simulations. It can be seen that the curves from automatic modelling using the three FE meshes (Mesh 1, Mesh 2 and Mesh 3) almost coincide up to the peak points, which indicates that the proposed criterion is mesh-objective. The

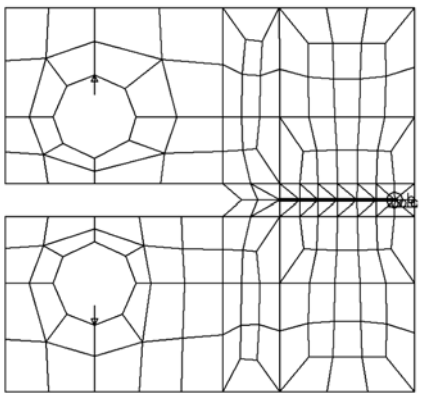

Fig.13 FE mesh with pre-inserted cohesive interface element (Mesh *P*)

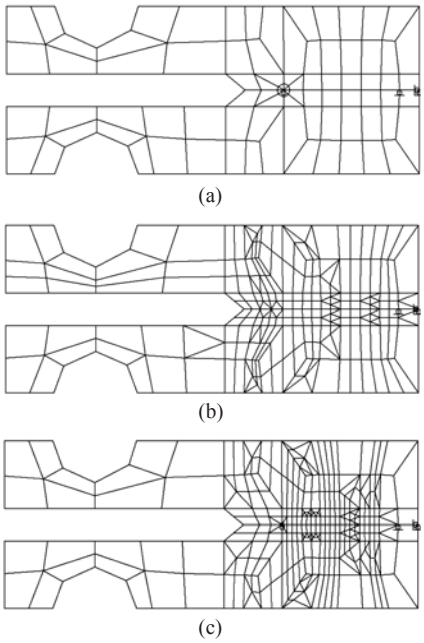

Fig.14 Initial FE meshes around the cracking line used in automatic crack propagation. (a) Mesh 1; (b) Mesh 2; (c) Mesh 3

response predicted by the method of pre-inserting CIEs is also very close to that of the automatic modelling approach. This demonstrates that the proposed criterion is able to correctly predict when a ductile crack propagates. The discrepancy between the test data and the numerical predictions may have been caused by a few factors: (i) the modelled boundary condition is not exactly the same as that in the test; (ii) the assumed σ-COD relation may be not the real one; and (iii) the criterion is based on the small deformation formulation (Eq.(8)) whereas the test specimen may have experienced finite deformation.

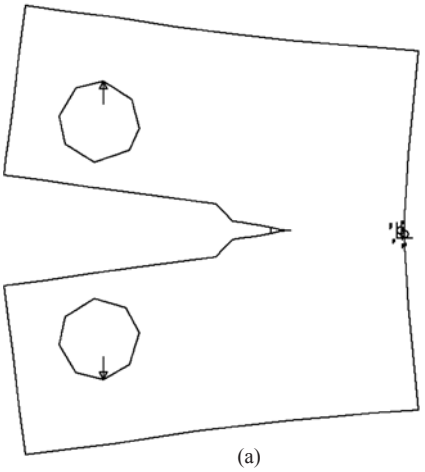

(a)

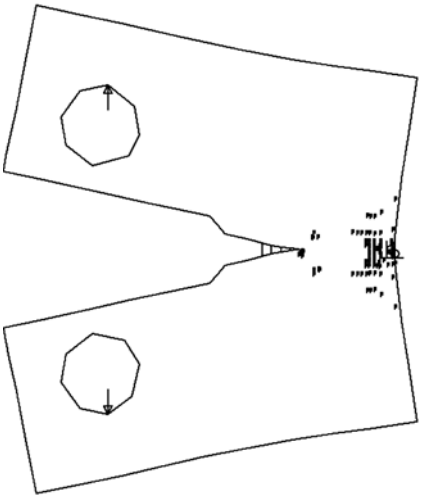

(b)

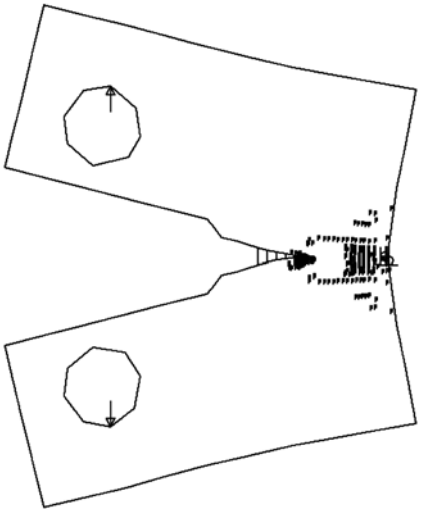

(c)

Fig.15 Evolution of cohesive crack zone and plasticity zone using Mesh 2 (displacement display scale=500). (a) F=4.5 kN; (b) F=6.5 kN; (c) F=7.19 kN (peak load)

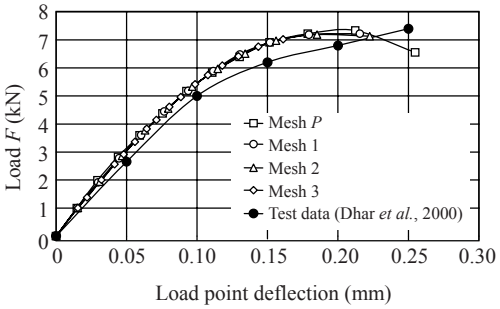

Fig.16 Load-load point deflection curves of the CT specimen

CONCLUSION

This paper has derived an explicit crack propagation criterion based on the Griffith energy concept and the CZM. The criterion has been implemented in an in-house finite element program based on the fully automatic discrete crack modelling methodology. Three examples were modelled to validate the proposed criterion. Good agreement between the numerical results and the experimental data has been observed.

It has been demonstrated that a unified numerical framework for modelling fracture in both quasi-brittle and ductile materials is possible due to the wide applicability of the proposed criterion. Much work remains to further validate it both experimentally and numerically, especially for multi-cracking problems and mixed-mode ductile cracking problems involving large yielding.

References

ACI Report 446.3R-97, 1997. Finite Element Analysis of Fracture in Concrete Structures: State-of-the-Art. Reported by ACI Committee 446.

Arrea, M., Ingraffea, A.R., 1982. Mixed-mode Crack Propagation in Mortar and Concrete. Report No. 81-13, Department of Structural Engineering, Cornell University, USA.

Bocca, P., Carpinteri, A., Valente, S., 1991. Mixed-mode fracture of concrete. *International Journal of Solid and Structures*, **27**(9):1139-1153. [doi:10.1016/0020-7683(91)90115-V]

Bresler, B., Scordelis, A.C., 1963. Shear strength of reinforced concrete beams. *Journal of the American Concrete Institute*, **60**(4):51-72.

Dhar, S., Dixit, P.M., Sethuraman, R., 2000. A continuum damage mechanics model for ductile fracture. *International Journal of Pressure Vessels and Piping*,

77(6):335-344. [doi:10.1016/S0308-0161(00)00019-3]

Griffith, A.A., 1921. The phenomena of rupture and flow in solids. *Philosophical Transactions of the Royal Society of London Series A*, 221:163-198.

Gurson, A.L., 1977. Continuum theory of ductile rupture by void nucleation and growth: Part I—yield criteria and flow rules for porous ductile media. *Journal of Engineering Materials Technology-Transactions of ASME*, **99**:2-15.

Hellen, T.K., 1975. On the method of virtual crack extension. *International Journal for Numerical Methods in Engineering*, **9**(1):187-207. [doi:10.1002/nme.1620090114]

Hillerborg, A., Rots, J., 1989. Crack concepts and numerical modelling, Report of the Technical Committee 90-FMA Fracture Mechanics to Concrete—applications, Elfgren, L. (Ed.), RILEM. Chapman and Hall, London, p.128-150.

Hillerborg, A., Modeer, M., Petersson, P.E., 1976. Analysis of crack formation and crack growth in concrete by means of fracture mechanics and finite elements. *Cement and Concrete Research*, **6**(6):773-782. [doi:10.1016/0008-8846(76)90007-7]

Li, H., Chandra, N., 2003. Analysis of crack growth and crack-tip plasticity in ductile materials using cohesive zone models. *International Journal of Plasticity*, **19**(6):849-882.

Li, W.Z., Siegmund, T., 2002. An analysis of crack growth in thin-sheet metal via a cohesive model. *Engineering Fracture Mechanics*, **69**(18):2073-2093. [doi:10.1016/S0013-7944(02)00013-9]

May, I.M., Duan, Y., 1997. A local arc-length procedure for strain softening. *Computers and Structures*, **64**(1-4):297-303. [doi:10.1016/S0045-7949(96)00172-1]

Petersson, P.E., 1981. Crack Growth and Development of Fracture Zone in Plain Concrete and Similar Materials. Report TVBM-1006, Division of Building Materials, Lund Institute of Technology, Lund, Sweden.

Rots, J., 1991. Smeared and discrete representations of localized fracture. *International Journal of Fracture*, **51**(1):45-59. [doi:10.1007/BF00020852]

Rots, J., de Borst, R., 1987. Analysis of mixed-mode fracture in concrete. *Journal of Engineering Mechanics ASCE*, **113**(11):1739-1758.

Siegmund, T., Brocks, W., 2000. Numerical study on the correlation between the work of separation and the dissipation rate in ductile fracture. *Engineering Fracture Mechanics*, **67**(2):139-154. [doi:10.1016/S0013-7944(00)00054-0]

Turner, C.E., Kolednik, O., 1994. A micro and macro approach to the energy-dissipation rate model of stable ductile crack-growth. *Fatigue & Fracture of Engineering Materials and Structures*, **17**(9):1089-1107. [doi:10.1111/j.1460-2695.1994.tb00837.x]

Tvergaard, V., Hutchinson, J.W., 1992. The relation between crack-growth resistance and fracture process parameters in elastic plastic solids. *Journal of the Mechanics and Physics of Solids*, **40**(6):1377-1397. [doi:10.1016/0022-5096(92)90020-3]

Tvergaard, V., Hutchinson, J.W., 1996. Effect of strain-dependent cohesive zone model on predictions of crack growth resistance. *International Journal of Solids and Structures*, **33**(20-22):3297-3308. [doi:10.1016/0020-7683(95)00261-8]

Xie, M., 1995. Finite Element Modelling of Discrete Crack Propagation, Ph.D Thesis, University of New Mexico, USA.

Xie, M., Gerstle, W.H., 1995. Energy-based cohesive crack propagation modelling. *Journal of Engineering Mechanics ASCE*, **121**(12):1349-1458. [doi:10.1061/(ASCE)0733-9399(1995)121:12(1349)]

Yang, Z.J., Chen, J.F., 2004. Fully automatic modelling of cohesive discrete crack propagation in concrete beams using local arc-length methods. *International Journal of Solids and Structures*, **41**(3-4):801-826. [doi:10.1016/j.ijsolstr.2003.09.033]

Yang, Z.J., Proverbs, D., 2004. A comparative study of numerical solutions to nonlinear discrete crack modelling of concrete beams involving sharp snap-back. *Engineering Fracture Mechanics*, **71**(1):81-105. [doi:10.1016/S0013-7944(03)00047-X]

Zhang, Z.L., Thaulow, C., Odegard, J., 2000. A complete Gurson model approach for ductile fracture. *Engineering Fracture Mechanics*, **67**(2):155-168. [doi:10.1016/S0013-7944(00)00055-2]